

Gyroscopic Stabilization of Launch Package in Induction Type Coilgun

Giancarlo Becherini

Abstract—The aim of this paper is to study the problem of gyroscopic stabilization of the launch package in induction type coilguns. This result can be obtained by utilizing a double-feed induction coilgun which provides rotation to the launch package while it is accelerating. Such launcher is comprised of two coils, one generating a travelling magnetic field (and consequently the axial acceleration) the other a rotating magnetic field for the rotation of the projectile. Electromagnetic analysis, based on a cylindrical sheet current model, allows one to determine, as a function of the two slips (in the translation motion and in the rotation motion) all the electric, magnetic and mechanical quantities. Thermal and mechanical stress are determined too. Finally the results for a launcher, in which a 2 kg projectile is accelerated, are reported. For this application time dependence of the principal electromechanical quantities are shown. A comparison with the same launcher running as a linear induction launcher is developed too.

Index Terms—Gyroscopic stabilization of the projectile, induction coilgun.

I. INTRODUCTION

THE LITERATURE contains multiple theoretical and experimental treatments of induction type coil-guns which discuss the advantages of electromagnetic launchers compared to conventional chemical launchers [1]–[5]. In a few papers, the problem of projectile stabilization during its in-bore flight [6]–[8] has been considered (problem of interior ballistics). This problem arises since the projectile is supported only by air and electromagnetic forces but not by any other physical means. We know of no paper where the stabilization of the trajectory of the launch package during its in-air flight is considered. In considering the question of projectile trajectory stabilization (i.e. the projectile must always maintain its own axis tangent to its trajectory), this paper analyzes the behavior of the projectile once it has left the barrel and is in free flight (problem of exterior ballistics). A solution is also proposed which, in our opinion, may have positive effects as well on the stabilization of the projectile within the barrel itself.

Historically the stabilization problem has been resolved in one of the following ways [9]:

- utilizing spherical projectiles;
- utilizing projectiles with an aerodynamic center of buoyancy behind the barycenter;
- utilizing gyroscopic stabilization.

Manuscript received December 17, 1999.

The author is with Accademia Navale, Viale Italia 72, 57100 Livorno, Italy (e-mail: simo@sysnet.it).

Publisher Item Identifier S 0018-9464(01)00205-9.

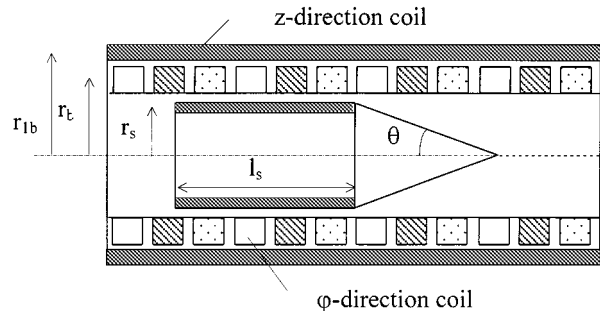


Fig. 1. Schematic representation of double-feed induction launcher.

We discard the first method because a spherical projectile has ballistic characteristics worse than cylindrical ones, the second because it needs fins on the terminal part of the projectile. The authors consider gyroscopic stabilization the best method for induction coilguns as it does not require projectiles constructed with particular characteristics; consequently, it is possible to use projectiles with the most desirable ballistic characteristics (e.g. to facilitate atmospheric entry). From the ballistic point of view the best performance is obtained by massive and long projectiles. Such projectiles have aerodynamic center of buoyancy before the barycenter and so they are inherently unstable [9].

Gyroscopic stabilization is obtained by a rotation of the launch package round the thrust axis with a speed greater than critical speed (such speed depends on dimensions and shape of the projectile).

In conventional launch systems, the projectile rotation is obtained by utilizing a rifled barrel with an opportune pitch. In induction coil-guns barrel-projectile contact is missing and so a different solution is necessary. In this paper a double-feed induction launcher (DFIL) is analyzed. Such launcher is equipped with two coils, as shown in Fig. 1. One of them is coiled in the ϕ -direction (as in a linear induction launcher) and produces translational motion, the other one is coiled in the z -direction (as in the stator of a polyphase induction motor) and produces the rotational motion.

The thickness of the sleeve conductor around the launch mass is chosen to be less than the penetration depth so that the current distribution is relatively uniform in the radial direction. In this way it is possible to reduce the actual current distribution, of both the sleeve and the barrel, to a cylindrical surface.

The analytical solution permits the determination of all electromechanical quantities. Consequently the thermal and mechanical stress in the sleeve can be determined too. Also the effects of the interference between the travelling and the rotating fields is considered, and the corresponding losses are calculated.

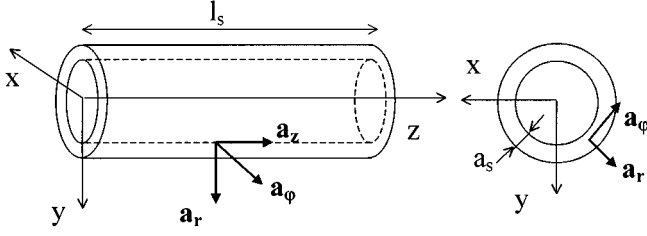


Fig. 2. Conductor sleeve and cylindrical coordinates.

In Fig. 2 the conductor sleeve and the cylindrical coordinates utilized in the analysis are represented.

II. GYROSCOPIC STABILIZATION

Stabilization of the projectile trajectory is achieved if the projectile rotates around its longitudinal axis (i.e. around the direction tangent to the trajectory) with an angular velocity greater than a critical velocity ω_{cr} obtained from (1) [9].

$$\omega_{cr} = \frac{2}{J} \sqrt{\frac{K_m}{C_r}} R \ell J_t \quad (1)$$

where:

$$R = C_r \rho S \frac{v^2}{2} \quad (2)$$

$$K_m = \frac{b}{\ell} (K_p + C_r) \quad (3)$$

In (1)–(3) the symbols are defined:

J	moment of inertia
J_t	transversal moment of inertia
ℓ	projectile length
R	aerodynamic drag
C_r	coefficient of aerodynamic drag
S	max projectile transversal section
ρ	air density
v	projectile velocity
K_p	aerodynamic lift gradient
b	distance between center of mass and center of aerodynamic buoyancy

III. MATHEMATICAL MODEL

The coil placed in the z -direction produces a magnetic field travelling with a synchronous speed v_{sz} while the coil placed in the φ -direction produces a magnetic field rotating with an angular synchronous speed ω_s (the corresponding tangential velocity is indicated with $v_{s\varphi}$). The synchronous speeds, with τ and β indicating the pole pitch and the wave number, respectively, with p the polar pair, and with r_s the mean radius of the sleeve, are:

$$v_{sz} = \frac{2\tau}{T} = \frac{\tau}{\pi} \omega_1 = \frac{\omega_1}{\beta} \quad (4)$$

$$\omega_s = \frac{2\pi f_2}{p} = \frac{\omega_2}{p} = \frac{v_{s\varphi}}{r_s} \quad (5)$$

Denoting with s_z , s_φ , v_z and v_φ the slips, and the speeds in the φ and z -directions, it is possible to write:

$$s_z = \frac{v_{sz} - v_z}{v_{sz}} \quad (6)$$

$$s_\varphi = \frac{v_{s\varphi} - v_\varphi}{v_{s\varphi}} \quad (7)$$

From (4)–(7), with ω_m indicating the rotation speed, the velocities in both directions are:

$$v_z = (1 - s_z)v_{sz} \quad (8)$$

$$v_\varphi = \omega_m r_s = (1 - s_\varphi)r_s \omega_s = (1 - s_\varphi)r_s \frac{\omega_2}{p} \quad (9)$$

Because the thickness of the sleeve in the radial direction is small the actual current distributions can be reduced to cylindrical surface current sheets. The same choice can be made for the current distributions in the barrel [10]. Under these hypotheses there are two surface current densities (A/m) in both the φ and z directions located at an effective radius r_b and r_{b1} , respectively, as shown in Fig. 1. Assuming a traveling-wave form and phasor notation, one can write:

$$\begin{aligned} \mathbf{K}_{b\varphi} &= K_{b\varphi} \cos(\omega_1 t - \beta z) \mathbf{a}_\varphi = \text{Re} \left\{ K_{b\varphi} e^{j(\omega_1 t - \beta z)} \right\} \mathbf{a}_\varphi \\ &= \text{Re} \{ \dot{K}_{b\varphi} \} \mathbf{a}_\varphi \end{aligned}$$

$$\begin{aligned} \mathbf{K}_{bz} &= K_{bz} \cos(\omega_2 t - \varphi) \mathbf{a}_z = \text{Re} \left\{ K_{bz} e^{j(\omega_2 t - \varphi)} \right\} \mathbf{a}_z \\ &= \text{Re} \{ \dot{K}_{bz} \} \mathbf{a}_z \end{aligned}$$

Neglecting the displacement current, the Laplacian of the magnetic vector potential \mathbf{A}_b is:

$$\nabla^2 \mathbf{A}_b = \nabla^2 A_{br} \mathbf{a}_r + \nabla^2 A_{b\varphi} \mathbf{a}_\varphi + \nabla^2 A_{bz} \mathbf{a}_z = 0 \quad (10)$$

Considering, furthermore, the relationships relative to flux density, electric field and sleeve surface current densities:

$$\begin{aligned} \mathbf{B} &= B_r \mathbf{a}_r + B_\varphi \mathbf{a}_\varphi + B_z \mathbf{a}_z \\ &= \left(\frac{\partial A_{bz}}{r \partial \varphi} - \frac{\partial A_{b\varphi}}{\partial z} \right) \mathbf{a}_r - \frac{\partial A_{bz}}{\partial r} \mathbf{a}_\varphi + \frac{1}{r} \frac{\partial (r A_{b\varphi})}{\partial r} \mathbf{a}_z \end{aligned} \quad (11)$$

$$\begin{aligned} \mathbf{E} &= E_r \mathbf{a}_r + E_\varphi \mathbf{a}_\varphi + E_z \mathbf{a}_z \\ &= \frac{\partial A_r}{\partial t} \mathbf{a}_r + \frac{\partial A_\varphi}{\partial t} \mathbf{a}_\varphi + \frac{\partial A_z}{\partial t} \mathbf{a}_z \end{aligned} \quad (12)$$

$$\mathbf{K}_s = \sigma_s a_s (\mathbf{E} + \mathbf{v} \times \mathbf{B}) \quad (13)$$

where a_s and σ_s are the sleeve thickness and the sleeve conductivity, respectively, and

$$\mathbf{v} = v_\varphi \mathbf{a}_\varphi + v_z \mathbf{a}_z \quad (14)$$

is the velocity, it is possible to obtain, as demonstrated in the Appendix, the components of flux density and surface current densities in the sleeve.

It is therefore possible to determine the force density (Pa) acting on the sleeve by the relation:

$$\begin{aligned} \mathbf{F} &= \mathbf{K}_s \times \mathbf{B}_r = F_r \mathbf{a}_\varphi + F_\varphi \mathbf{a}_r + F_z \mathbf{a}_z \\ &= (K_{s\varphi} B_{sz} - K_{sz} B_{s\varphi}) \mathbf{a}_r + K_{sz} (B_{r\varphi} + B_{rz}) \mathbf{a}_\varphi \\ &\quad - K_{s\varphi} (B_{r\varphi} + B_{rz}) \mathbf{a}_z \end{aligned} \quad (15)$$

In phasor notation, denoting with $\dot{K}_{s\varphi}^*$ and \dot{K}_{sz}^* the complex conjugates of $\dot{K}_{s\varphi}$ and \dot{K}_{sz} , the mean values of the force densities in the r , φ , and z , are:

$$F_r = -\frac{1}{2} \text{Re} \left\{ \dot{K}_{s\varphi}^* \dot{B}_z - \dot{K}_{sz}^* \dot{B}_\varphi \right\} \quad (16)$$

$$F_\varphi = -\frac{1}{2} \text{Re} \left\{ \dot{K}_{s\varphi}^* \dot{B}_{r\varphi} \right\} \quad (17)$$

$$F_z = \frac{1}{2} \text{Re} \left\{ \dot{K}_{sz}^* \dot{B}_{rz} \right\} \quad (18)$$

Sending excitation current in only one of the two windings, indicating with $F_{r\varphi}$ and F_{rz} the components of radial force obtained by feeding singularly the φ -direction or the z -direction winding, one finds:

$$F_{r\varphi} = \frac{\beta r_b^2 \mu_0^2 K_1^2(\beta r_b) s_z}{2r_s K_1(\beta r_s)(s_z^2 + s_z^{*2})} \times \left[\frac{K_0(\beta r_b) I_1(\beta r_s) s_z^*}{K_1(\beta r_s)} + I_0(\beta r_b) s_z \right] K_{b\varphi}^2 \quad (19)$$

$$F_{rz} = \frac{\mu_0 s_\varphi s_\varphi^* K_{bz}^2}{4(s_\varphi^2 + s_\varphi^{*2})} \quad (20)$$

$$F_\varphi = \frac{s_\varphi s_\varphi^*}{s_\varphi^2 + s_\varphi^{*2}} \frac{\mu_0 K_{bz}^2}{4} \quad (21)$$

$$F_z = \frac{s_z s_z^*}{s_z^2 + s_z^{*2}} \frac{\mu_0 \beta r_b^2 K_1^2(\beta r_b) I_1(\beta r_s)}{2r_s K_1(\beta r_s)} K_{b\varphi}^2 \quad (22)$$

If the coils are contemporaneously fed the surface current densities and the force densities become:

$$\dot{K}'_{s\varphi} = \dot{K}_{s\varphi} + a_s \sigma_s v_z \dot{B}_{rz} \quad (23)$$

$$\dot{K}'_{sz} = \dot{K}_{sz} - a_s \sigma_s v_\varphi \dot{B}_{r\varphi} \quad (24)$$

The new force densities are:

$$F'_r = F_{r\varphi} + F_{rz} \quad (25)$$

$$F'_\varphi = F_\varphi - a_s \sigma_s v_z B_{r\varphi}^2 \quad (26)$$

$$F'_z = F_z - a_s \sigma_s v_\varphi B_{rz}^2 \quad (27)$$

Equation (27) shows that the force developed with a double-feed launcher is smaller than the one produced with a LIL. This is the price to obtain the rotation; this price has to be paid also in conventional chemical guns in which the rifled barrel determines energy loss.

The propulsive force (N) and the torque (Nm) which determines the rotation are:

$$F_s = 2\pi r_s l_s F'_z \quad (28)$$

$$T = 2\pi r_s^2 l_s F'_\varphi \quad (29)$$

IV. EQUATIONS OF MOTION

Under the hypothesis that the motion inside the barrel has the same characteristics it has in free air motion, the aerodynamic drag can be evaluated by relation (2).

Neglecting the viscous drag relative to the rotation motion and denoting with m the total mass the equations of motion result:

$$F_s = m \frac{dv_z}{dt} + R \quad T = J \frac{d\omega_m}{dt}$$

Considering (8) and (9), the above equations can be written as:

$$F_s = -mv_{sz} \frac{ds_z}{dt} + C_r \rho S v_{sz}^2 (1 - s_z)^2 \quad (30)$$

$$T = -J\omega_s \frac{ds_\varphi}{dt} \quad (31)$$

V. ENERGY LOSS IN THE SLEEVE

The Joule power loss in the sleeve, denoting with J_s the current density (A/m^2), can be calculated by the following equation:

$$p_{\text{joule}} = \frac{1}{\sigma_s} \int_v J_s^2 dv = \frac{1}{\sigma_s a_s^2} \int_v (K_{s\varphi}^2 + K_{sz}^2) dv. \quad (32)$$

Denoting with l_s the sleeve length, (32) becomes:

$$p_{\text{joule}} = \frac{2\pi r_s l_s}{\sigma_s a_s} (K_{s\varphi}^2 + K_{sz}^2). \quad (33)$$

The energy loss in the sleeve is:

$$E_{\text{joule}} = \int_{t_1}^{t_2} p_{\text{joule}} dt = \int_{t_1}^{t_2} \frac{2\pi r_s l_s}{\sigma_s a_s} (K_{s\varphi}^2 + K_{sz}^2) dt. \quad (34)$$

The energy efficiency (neglecting the energy loss due to viscous friction) is defined as the ratio between the projectile's kinetic energy and the total energy supplied to the projectile. When the launcher works as a LIL the efficiency is:

$$\eta = \frac{\frac{1}{2} m v_z^2}{E_{\text{joule}} + \frac{1}{2} m v_z^2}. \quad (35)$$

For a double-feed launcher, the efficiency is:

$$\eta = \frac{\frac{1}{2} m v_z^2 + \frac{1}{2} J \omega_m^2}{E_{\text{joule}} + \frac{1}{2} m v_z^2 + \frac{1}{2} J \omega_m^2}. \quad (36)$$

The energy loss produces a rise in the sleeve temperature. Considering an adiabatic process the sleeve temperature can be determined as:

$$\vartheta = \vartheta_1 + \int_{t_1}^t \frac{2\pi r_s l_s}{m c \sigma_s} (K_{s\varphi}^2 + K_{sz}^2) dt \quad (37)$$

where ϑ_1 is the initial temperature.

VI. APPLICATION

In this section we report the results of a numerical example in which the projectile is constituted by a cylindrical part, surrounded by a sleeve, ending with a conical part, as shown in Fig. 1, having $\theta = 10^\circ$. Parameter values follow:

Sleeve radius	$r_s = 5$ cm
Sleeve length	$l_s = 25$ cm
Sleeve thickness	$a_s = 5$ mm
Gap length	$t = 5$ mm
Barrel radius	$r_b = 6$ cm
Aluminum density	$\gamma_{al} = 2700$ Kg/m ³
Mass of launch package	$m = 2$ kg
Moment of inertia	$J = 0.025$ kgm ²
Transversal moment of inertia	$J_t = 0.0031$ kgm ²
Aerodynamic lift gradient	$K_p = 0.035$
Air density	$\rho = 1.29$ Kg/m ³
Coeff. of aerodynamic drag	$C_r = 0.35$
Aluminum specific heat	$c = 908$ J/kg °C
Aluminum conductivity	$\sigma = 1.63 \times 10^7$ S/m
Aluminum stress limit	$\sigma_m = 6.9 \times 10^7$ Pa
Fusion temperature	$\vartheta_f = 658^\circ\text{C}$

The coefficient of aerodynamic drag changes with the speed; it is quasiconstant for $M(\text{Mach}) < 1$, it increases rapidly around 1 then decreases slowly [9]. For the aim of this work it is sufficient to assume for C_r a constant mean value equal to

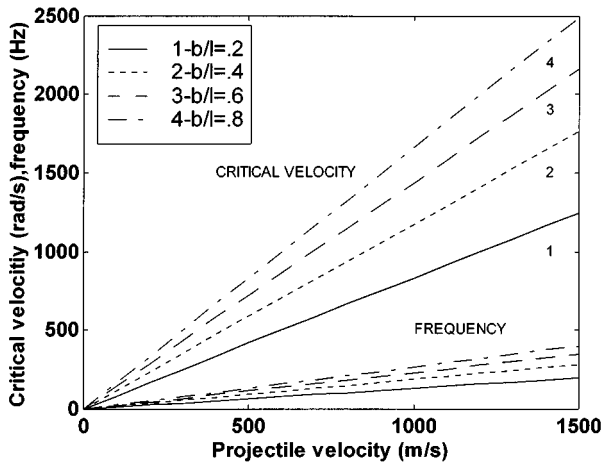


Fig. 3. Trends of critical angular velocity, and corresponding frequency, as a function of the translation velocity, for some values of the ratio b/ℓ .

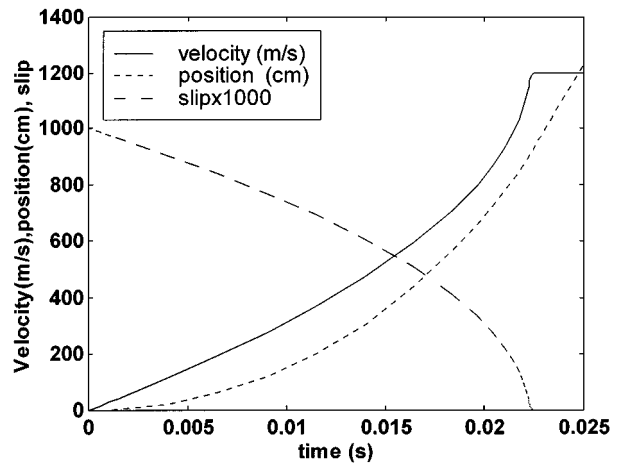


Fig. 5. Slip, velocity and projectile position as function of the time.

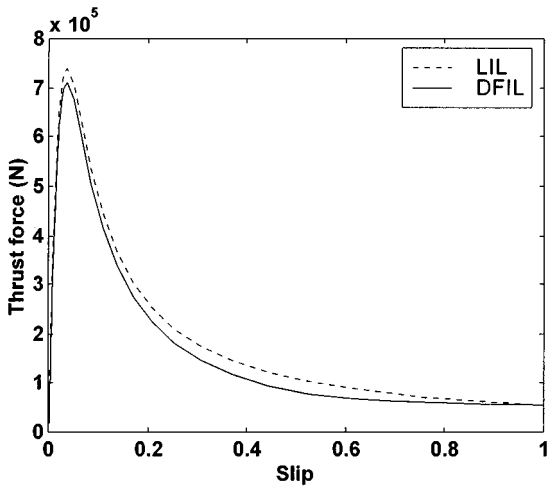


Fig. 4. Trends of the thrust, as a function of the slip, for a launcher working as a LIL and as DFIL.

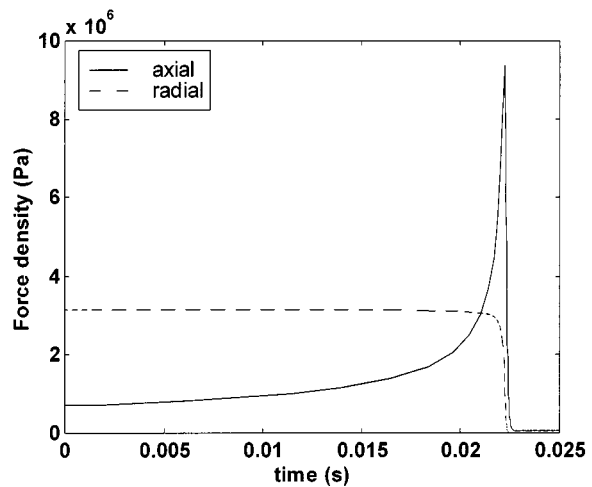


Fig. 6. Axial and radial force densities as a function of the time for the LIL.

0.35. From (1) it is possible to determine the critical angular velocity of the projectile. Fig. 3 depicts the trends in that velocity, and those of the corresponding frequency, as a function of the translation speed, for some values of the ratio b/ℓ .

The following results are obtained assuming $K_{b\varphi} = 12$ MA/m, $f_1 = 2$ kHz, $K_{bz} = 0.7$ MA/m, $f_2 = 300$ Hz.

Fig. 4 shows the trends of the thrust force, as a function of the slip, for the same launcher working as a LIL or as a DFIL. The DFIL's thrust is lower than the LIL's thrust owing to the braking force due to the fed z -direction coil.

Figs. 5 and 6 show the performance of a launcher utilized as a LIL. Fig. 5 shows that the 2 Kg projectile can be accelerated to 1.2 Km/s in about 22 ms with a barrel length 9.2 m.

Fig. 6 represents the force densities in the axial and radial directions. These densities have maximum values 9.5×10^6 Pa and 3.2×10^6 Pa, respectively. During the launching time the sleeve temperature increases 580°C . The efficiency defined by (35) is 51%.

The trends of force densities in all directions, when the launcher is running as a DFIL, are shown in Fig. 7. This picture confirms a small variation of the propulsive force density (see also Fig. 4) compared to the LIL's performance. The radial force density is practically invariant too. The tangential force

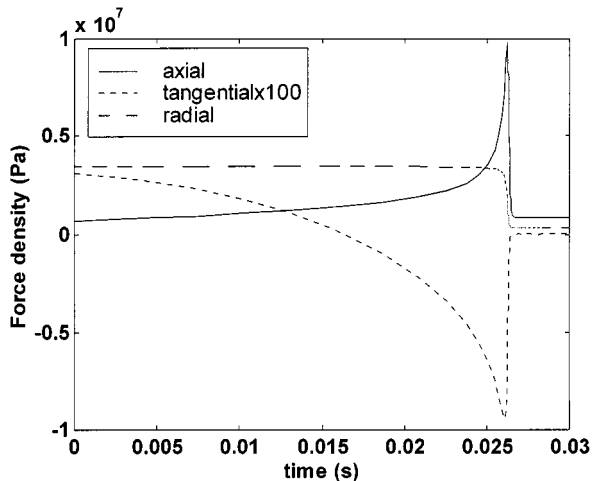


Fig. 7. Axial, radial and tangential force densities as a function of the time for the DFIL.

density has an initial value of 3×10^6 Pa, then it decreases and becomes negative (i.e. a braking force) when the time is greater than 16 ms.

Fig. 8 shows the trends of translation velocity, angular velocity, critical velocity, position of the projectile and of the slips

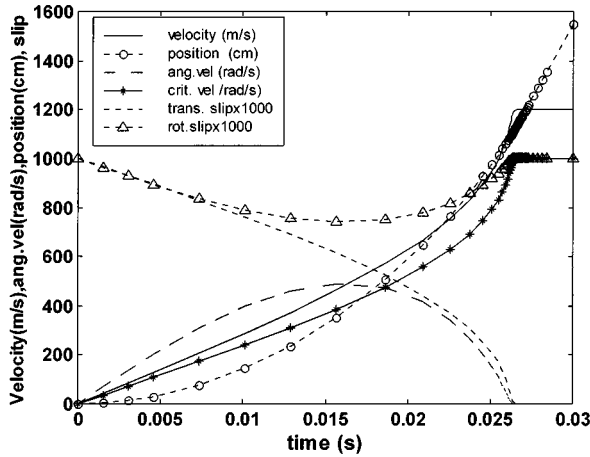


Fig. 8. Velocity, position, angular velocity, critical velocity and slips as a function of the time.

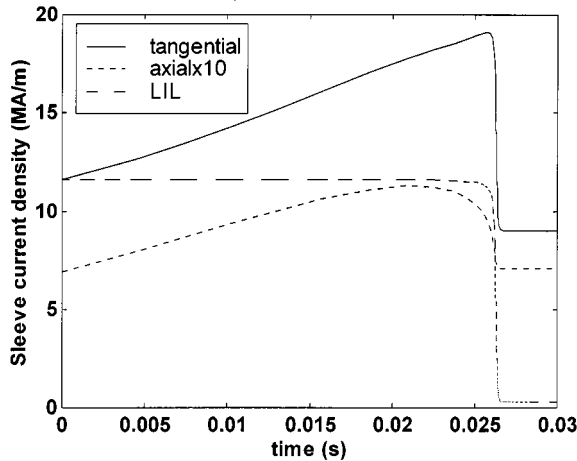


Fig. 9. Trends of the current densities in the sleeve.

in both directions of motion. Because the angular velocity can't be less than the critical one, the maximum projectile velocity is about 600 m/s corresponding to 19 ms. The angular velocity is 500 rad/s and the barrel length is 5 m.

The sleeve temperature increase is about 700°C and the efficiency, calculated by (36) is 33%. The sleeve's higher temperature and lower efficiency obtained with the DFIL is a consequence of the additional current in the z -direction coil; this current increases Joule losses and produces a braking action on the projectile. These results are confirmed also by Fig. 9 in which the actual sleeve current is compared with that related to a LIL.

Fig. 10 shows the trends of the same quantities represented in Fig. 8, but here the coils are fed sequentially. That is, the launch period is divided into two phases: in the first one only the z -direction coil is fed (therefore the projectile rotates), in the second one only the φ -direction is fed and so the projectile acquires a motion of translation. In the last phase the angular speed decreases as a consequence of the braking action due to the fed coil (the energy loss in the actual case is 4.13 kJ). In this case the maximum translation velocity is about 600 m/s, launch time 16 ms, barrel length 4.2 m. It is also found that the temperature increase 420°C, and the efficiency is about 51%.

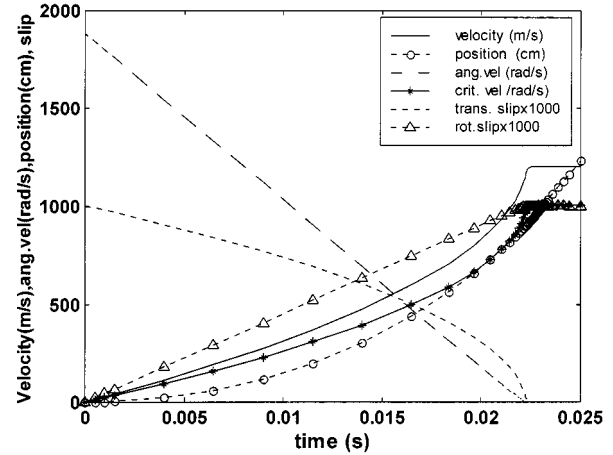


Fig. 10. Velocity, position, angular velocity, critical velocity and slips as a function of the time. Trends obtained feeding the coils at different times.

During the first phase the Joule loss is of 4.2 kJ and temperature increases less than 5°C. Therefore it can be affirmed that the first phase doesn't produce significant effects on efficiency and on material stress.

VII. CONCLUSIONS

On the assumption that a quasisteady state prevails during the operation of the coilgun (i.e. the mechanical time constants are much larger than the electrical ones) this paper provides the electromagnetic analysis of the DFIL along with a comparison with a LIL. The DFIL permits one to stabilize the trajectory of the projectile while it is flying; this is the important advantage compared to the LIL. There are however the following disadvantages:

- constructive complications in the realization of the coils;
- interference between the travelling and rotating magnetic field. This produces an effective reduction in the developed thrust force;
- because the angular speed must be greater than the critical speed the muzzle velocity must be lower;
- energy must be expended to rotate the projectile;
- energy losses are greater, and the efficiency is worse, owing to the braking effect caused by electromagnetic interferences;
- mechanical and thermal stresses are higher.

In the specific application it has been found advantageous to provide rotation to the projectile before it is accelerated. In such case the muzzle velocity is the same as the one obtained in simultaneous operation of both coils, but the mechanical and thermal stresses are lower and the efficiency is higher.

APPENDIX

Considering null the \mathbf{A}_b component in the radial direction, in (10), one can write:

$$\nabla^2 A_{b\varphi} \mathbf{a}_\varphi = \frac{1}{r} \frac{\partial}{\partial r} \left(r \frac{\partial A_{b\varphi} \mathbf{a}_\varphi}{\partial r} \right) + \frac{1}{r^2} \frac{\partial^2 A_{b\varphi} \mathbf{a}_\varphi}{\partial \varphi^2} + \frac{\partial^2 A_{b\varphi} \mathbf{a}_\varphi}{\partial z^2} = 0 \quad (1a)$$

$$\nabla^2 A_{bz} \mathbf{a}_z = \frac{1}{r} \frac{\partial}{\partial r} \left(r \frac{\partial A_{bz} \mathbf{a}_z}{\partial r} \right) + \frac{1}{r^2} \frac{\partial^2 A_{bz} \mathbf{a}_z}{\partial \varphi^2} + \frac{\partial^2 A_{bz} \mathbf{a}_z}{\partial z^2} = 0 \quad (2a)$$

By substitution of the following equations:

$$\begin{aligned} \mathbf{A}_{b\varphi} &= A_{b\varphi} \cos(\omega_1 t - \beta z + \gamma_\varphi) \mathbf{a}_\varphi \\ &= \text{Re} \left\{ A_{b\varphi} e^{j(\omega_1 t - \beta z + \gamma_\varphi)} \right\} \mathbf{a}_\varphi = \text{Re} \left\{ \dot{A}_{b\varphi} \right\} \mathbf{a}_\varphi \end{aligned} \quad (3a)$$

$$\begin{aligned} \mathbf{A}_{bz} &= A_{bz} \cos(\omega_2 t - \varphi + \gamma_z) \mathbf{a}_z \\ &= \text{Re} \left\{ A_{bz} e^{j(\omega_2 t - \varphi + \gamma_z)} \right\} \mathbf{a}_z = \text{Re} \left\{ \dot{A}_{bz} \right\} \mathbf{a}_z \end{aligned} \quad (4a)$$

the previous equations become:

$$\frac{d^2 A_{b\varphi}(r)}{dr^2} + \frac{1}{r} \frac{dA_{b\varphi}(r)}{dr} - \left(\beta^2 + \frac{1}{r^2} \right) A_{b\varphi}(r) = 0 \quad (5a)$$

$$r^2 \frac{d^2 A_{bz}(r)}{dr^2} + r \frac{dA_{bz}(r)}{dr} - A_{bz}(r) = 0 \quad (6a)$$

The solution of (5a) and (6a) are [11]:

$$A_{b\varphi}(r) = C_1 I_1(\beta r) + C_2 K_1(\beta r) \quad (7a)$$

$$A_{bz}(r) = C_3 r + \frac{C_4}{r} \quad (8a)$$

where I_1 and K_1 are modified Bessel functions.

With boundary conditions:

$$A_{bz}(\infty) = 0 \quad A_{b\varphi}(\infty) = 0$$

$$A_{bz}(0) = \text{finite} \quad A_{b\varphi}(0) = \text{finite}$$

$$B_{bz}(r_b^-) - B_{bz}(r_b^+) = \mu_0 K_{bz}$$

$$B_{b\varphi}(r_{1b}^-) - B_{b\varphi}(r_{1b}^+) = \mu_0 K_{b\varphi}$$

$$B_{br}(r_b^+) = B_{br}(r_b^-) \quad B_{br}(r_{1b}^+) = B_{br}(r_{1b}^-)$$

it is found that:

$$-r \geq r_b (r \geq r_{1b})$$

$$\dot{A}_{b\varphi} = \dot{K}_{b\varphi} r_b \mu_0 I_1(\beta r_b) K_1(\beta r) \quad (9a)$$

$$\dot{A}_{bz} = \frac{\mu_0 \dot{K}_{bz} r_{1b}^2}{2r} \quad (10a)$$

$$\dot{B}_{br} = -j \frac{\mu_0 \dot{K}_{bz} r_b^2}{2r^2} + j r_b \mu_0 \beta \dot{K}_{b\varphi} I_1(\beta r_b) K_1(\beta r) \quad (11a)$$

$$\dot{B}_{b\varphi} = \frac{\mu_0 \dot{K}_{bz} r_{1b}^2}{2r^2} \quad (12a)$$

$$\dot{B}_{bz} = -r_b \mu_0 \dot{K}_{b\varphi} \beta I_1(\beta r_b) K_0(\beta r) \quad (13a)$$

$$-r \leq r_b (r \leq r_{1b})$$

$$\dot{A}_{b\varphi} = r_b \mu_0 \dot{K}_{b\varphi} K_1(\beta r_b) I_1(\beta r) \quad (14a)$$

$$\dot{A}_{bz} = \frac{1}{2} \mu_0 \dot{K}_{bz} r \quad (15a)$$

$$\dot{B}_{br} = -j \frac{1}{2} \mu_0 \dot{K}_{bz} + j r_b \mu_0 \dot{K}_{b\varphi} K_1(\beta r_b) \beta I_1(\beta r) \quad (16a)$$

$$\dot{B}_{b\varphi} = -\frac{1}{2} \mu_0 \dot{K}_{bz} \quad (17a)$$

$$\dot{B}_{bz} = r_b \mu_0 \dot{K}_{b\varphi} \beta K_1(\beta r_b) I_0(\beta r) \quad (18a)$$

Similarly, imposing at the effective radius r_s of the sleeve, as shown in Fig. 1, the (unknown) surface current densities in the φ and z directions

$$\begin{aligned} \mathbf{K}_{s\varphi} &= K_{s\varphi} \cos(\omega_1 t - \beta z + \alpha_\varphi) \mathbf{a}_\varphi \\ &= \text{Re} \left\{ K_{s\varphi} e^{j(\omega_1 t - \beta z + \alpha_\varphi)} \right\} \mathbf{a}_\varphi \\ &= \text{Re} \left\{ \dot{K}_{s\varphi} \right\} \mathbf{a}_\varphi \end{aligned} \quad (19a)$$

$$\begin{aligned} \mathbf{K}_{sz} &= K_{sz} \cos(\omega_2 t - p\varphi + \alpha_z) \mathbf{a}_z \\ &= \text{Re} \left\{ K_{sz} e^{j(\omega_2 t - p\varphi + \alpha_z)} \right\} \mathbf{a}_z \\ &= \text{Re} \left\{ \dot{K}_{sz} \right\} \mathbf{a}_z \end{aligned} \quad (20a)$$

for the regions external to the sleeve in which $r \geq r_s$ and for those internal where $r \leq r_s$, one finds:

$$-r \geq r_s \quad \dot{A}_{s\varphi} = \dot{K}_{s\varphi} r_s \mu_0 I_1(\beta r_s) K_1(\beta r) \quad (21a)$$

$$\dot{A}_{sz} = \frac{\mu_0 \dot{K}_{sz} r_s^2}{2r} \quad (22a)$$

$$\dot{B}_{sr} = -j \frac{\mu_0 \dot{K}_{sz} r_s^2}{2r^2} + j \beta r_s \mu_0 \dot{K}_{s\varphi} I_1(\beta r_s) K_1(\beta r) \quad (23a)$$

$$\dot{B}_{s\varphi} = \frac{\mu_0 \dot{K}_{sz} r_s^2}{2r^2} \quad (24a)$$

$$\dot{B}_{sz} = -\beta r_s \mu_0 \dot{K}_{s\varphi} I_1(\beta r_s) K_0(\beta r) \quad (25a)$$

$$-r \leq r_s$$

$$\dot{A}_{s\varphi} = r_s \mu_0 \dot{K}_{s\varphi} K_1(\beta r_s) I_1(\beta r) \quad (26a)$$

$$\dot{A}_{sz} = \frac{1}{2} \mu_0 \dot{K}_{sz} r \quad (27a)$$

$$\dot{B}_{sr} = -j \frac{1}{2} \mu_0 \dot{K}_{sz} + j \beta r_s \mu_0 \dot{K}_{s\varphi} K_1(\beta r_s) I_1(\beta r) \quad (28a)$$

$$\dot{B}_{s\varphi} = -\frac{1}{2} \mu_0 \dot{K}_{sz} \quad (29a)$$

$$\dot{B}_{sz} = \beta r_s \mu_0 \dot{K}_{s\varphi} K_1(\beta r_s) I_0(\beta r) \quad (30a)$$

The φ and z -components of the electric field expressed by (12), deriving the magnetic vector potential and calculating in $r = r_s$, where the cylindrical surface current sheets are applied, can be written in phasor form as follows:

$$\dot{E}_\varphi = \dot{E}_{b\varphi} + \dot{E}_{s\varphi} = -j\omega_1 (\dot{A}_{b\varphi} + \dot{A}_{s\varphi}) \quad (31a)$$

$$\dot{E}_z = \dot{E}_{bz} + \dot{E}_{sz} = -j\omega_2 (\dot{A}_{bz} + \dot{A}_{sz}) \quad (32a)$$

From (13) the surface current density in the sleeve can be found. Sending excitation current in only one of the two windings [feeding only the φ -direction coil, the system works as a linear induction launcher (LIL); feeding only the z -direction coil, the system works as an asynchronous induction motor], the φ and z -components of the surface current densities in the sleeve are, in phasor form:

$$\dot{K}_{s\varphi} = a_s \sigma_s (\dot{E}_\varphi + v_z \dot{B}_{r\varphi}) \quad (33a)$$

$$\dot{K}_{sz} = a_s \sigma_s (\dot{E}_z - v_\varphi \dot{B}_{rz}) \quad (34a)$$

where $\dot{B}_{r\varphi}$ and \dot{B}_{rz} are the radial flux densities produced by the currents in φ -direction and z -direction. Define:

$$s_z^* = \frac{1}{a_s \sigma_s \mu_0 \beta r_s v_{sz} K_1(\beta r_s) I_1(\beta r_s)} \quad (35a)$$

$$s_\varphi^* = \frac{1}{\frac{\mu_0}{2} \omega a_s \sigma_s r_s} \quad (36a)$$

as the critical slips at which the propulsive forces reach their maximum value. Setting moreover:

$$\theta_z = tg^{-1} \frac{s_z^*}{s_z} \quad \theta_\varphi = tg^{-1} \frac{s_\varphi^*}{s_\varphi} \quad (37a)$$

it results that:

$$\begin{aligned} \dot{B}_{r\varphi} &= \dot{B}_{br\varphi} + \dot{B}_{sr\varphi} \\ &= \frac{\beta r_b \mu_0 K_1(\beta r_b) I_1(\beta r_s) s_s^* e^{j\theta_z} \dot{K}_{b\varphi}}{\sqrt{s_z^2 + s_z^{*2}}} \end{aligned} \quad (38a)$$

$$\dot{B}_{rz} = \dot{B}_{brz} + \dot{B}_{srz} = \frac{-\mu_0 s_\varphi^* e^{j\theta_\varphi} \dot{K}_{bz}}{2\sqrt{s_\varphi^2 + s_\varphi^{*2}}} \quad (39a)$$

$$\dot{B}_\varphi = \dot{B}_{b\varphi} + \dot{B}_{s\varphi} = -\frac{\mu_0}{2} \left(1 + \frac{s_\varphi^* e^{j\theta_\varphi}}{\sqrt{s_\varphi^2 + s_\varphi^{*2}}} \right) \dot{K}_{bz} \quad (40a)$$

$$\begin{aligned} \dot{B}_z &= \dot{B}_{bz} + \dot{B}_{sz} \\ &= \beta r_b \mu_0 K_1(\beta r_b) \\ &\quad \cdot \left[\frac{s_z^* K_0(\beta r_b) I_1(\beta r_s) e^{j\theta_z}}{K_1(\beta r_s) \sqrt{s_z^2 + s_z^{*2}}} + I_0(\beta r_s) \right] \dot{K}_{b\varphi} \end{aligned} \quad (41a)$$

$$\dot{K}_{s\varphi} = \frac{-s_z r_b K_1(\beta r_b) e^{j\theta_z} \dot{K}_{b\varphi}}{r_s K_1(\beta r_s) \sqrt{s_z^2 + s_z^{*2}}} \quad (42a)$$

$$\dot{K}_{sz} = \frac{-s_\varphi e^{j\theta_\varphi} \dot{K}_{bz}}{\sqrt{s_\varphi^2 + s_\varphi^{*2}}} \quad (43a)$$

REFERENCES

- [1] J. L. He, E. Levi, Z. Zabar, and L. Birembaum, "Concerning the design of capacitively driven induction gun," *IEEE Trans. Plasma Sci.*, vol. 17, June 1989.
- [2] Z. Zabar, Y. Naot, L. Birembaum, E. Levi, and P. N. Joshi, "Design and power conditioning for the coil-gun," *IEEE Trans. Magn.*, vol. 25, January 1989.
- [3] A. Andrews, "Coilgun structures," *IEEE Trans. on Magn.*, vol. 29, January 1993.
- [4] G. Becherini, M. Raugi, and A. Tellini, "Thermal and mechanical stress in induction coilguns," *IEEE Trans. Magn.*, vol. 35, January 1999.
- [5] S. W. Sun, Y. M. Zhu, J. J. Cheng, and D. M. Wang, "The test and analysis of a 3-stage reconnection coilgun," *IEEE Trans. Magn.*, vol. 35, January 1999.
- [6] K. B. Kim, Z. Zabar, E. Levi, and L. Birembaum, "In-bore projectile dynamics in the linear induction launcher (LIL), Part I: Oscillations," *IEEE Trans. Magn.*, vol. 31, January 1995.
- [7] —, "In-bore projectile dynamics in the linear induction launcher (LIL), Part II: balloting, spinning, and nutation," *IEEE Trans. Magn.*, vol. 31, January 1995.
- [8] Musolino, M. Raugi, and B. Tellini, "3-D field analysis in tubular induction launchers with armature transverse motion: Thermal and mechanical stress in induction coilguns," *IEEE Trans. Magn.*, vol. 35, January 1999.
- [9] Pignone and Vercelli, *Appunti di balistica*. Firenze: Olimpia, 1987.
- [10] J. H. He, E. Levi, Z. Zabar, L. Birembaum, and Y. Naot, "Analysis of induction-type coilgun performance based on cylindrical current sheet model," *IEEE Trans. Magn.*, vol. 27, June 1991.
- [11] L. Gatteschi, *Funzioni speciali*. Torino: UTET, 1973.